Calcium phosphate/polyvinyl acetate coatings on SS304 ~~by~~ via galvanic co-deposition for orthopedic implant applications

I. Mendolia[1], C. Zanca[1], F. Ganci[1], G. Conoscenti[1], F. Carfì Pavia[1], V. Brucato[1,2], V. La Carrubba[1,2,3], F. Lopresti[1], S. Piazza[1], C. Sunseri[1], R. Inguanta[1,2*]

[1]Dipartimento di Ingegneria, Università di Palermo, Viale delle Scienze - 90128 Palermo (Italy)

[2]INSTM Palermo Research Unit, Viale delle Scienze - 90128 Palermo (Italy)

[3]ATeN Center, Università di Palermo, Viale delle Scienze - 90128 Palermo (Italy)

[*]Corresponding Author E-mail Address: rosalinda.inguanta@unipa.it

Formatted: Italian (Italy)

Abstract

In this work, the galvanic deposition method ~~was~~ is used to deposit coatings of brushite/hydroxyapatite/polyvinyl acetate on 304 stainless steel. ~~–~~Coatings ~~were~~ are obtained at different temperatures and with different sacrificial anodes, ~~and~~ ~~consist~~consisting of a mixture of brushite and hydroxyapatite. Samples ~~were~~ are aged in ~~the~~ a simulated body fluid (SBF), where a ~~completely~~complete conversion of brushite into hydroxyapatite with a simultaneous change in morphology and wettability occurred. The ~~C~~corrosion tests show~~ed~~ that, ~~in comparison~~ compared with bare 304, the coating shifts E_{corr} to anodic values and reduces i_{corr} $E_{corr,}$ and i_{corr} ~~have~~has different values at different aging times~~,~~ due to chemical interactions at the solid/liquid interface. The best performing deposits are those obtained by using Al as the sacrificial anode. The metal ~~ions~~ion release, measured after 21 days of aging, is very low and is attributable to the presence of a coating that slows~~-down~~ the steel corrosion. Coating cytotoxicity ~~was~~ is investigated through cell viability assays with MC3T3-E1 osteoblastic cells. ~~Results a~~ The results reveal~~ed~~ a high cytocompatibility~~,~~ comparable to ~~the~~that of a pure cell culture medium.

Formatted: Highlight

Keywords: Galvanic deposition, hydroxyapatite, orthopedic implants, polyvinyl acetate,

corrosion, cytotoxicity.

Introduction

The ~~fracture~~ fracturing of a bone~~,~~ due to various types of traumas or natural aging~~,~~ is a typical ~~way~~method of "failure" ~~of~~ for this tissue. Bone fracture is repaired ~~via~~ by the application of a temporary or permanent implant, which is still a challenge for orthopedic surgeons. This is especially true in the case of permanent implants that must be ~~long time~~ durable for a long time to ensure a high quality of ~~the patient~~ life [1]. For this reason, much attention ~~was~~ has been devoted to the continuous improvement of biomedical implants, whose global market has been estimated ~~in~~to be over 200 billion ~~euro~~euros with an annual increase of ~~about~~approximately 8% [2]. Medical devices must be fabricated with biomaterials that must be osteogenic, osteoinductive, osteoconductive, completely biocompatible, and non-toxic to avoid immunological problems [3,4]. In orthopedic applications, the most promising biomaterials are ~~the~~ bioactive glasses [5] and hydroxyapatite (HA) [6,7]. HA is a calcium phosphate compound (chemical formula $Ca_5(PO_4)_3(OH)$) with excellent biocompatibility properties due to its close similarity to ~~the~~ human bone tissues, both in terms of morphology and composition [8][9][10][11]. Unfortunately, HA does not exhibit the elastic and mechanical properties required to replace bone functionality. Thus, the most common use of HA consists ~~in~~of coating ~~of~~ mechanically resistant metallic substrates, such as titanium, magnesium alloys or steel [12]. In ~~the~~ body ~~fluid~~fluids, metallic ~~substrate is~~substrates are subjected to corrosion phenomena, leading to the release of irritating or toxic metal ions into the human body [13]. ~~Besides~~ In addition, the metals used in the biomedical field are also characterized by

poor osteointegration (an intimate union between a bone and an artificial implant without an apparent connective tissue)~~,~~ and cytotoxicity (~~effect of~~ a chemical, physical or biological effect capable of inducing damage to a cell) [2,14,15].

The use of metallic ~~substrate~~substrates coated with HA allows one to overcome the limits of single materials. ~~Particularly~~In particular, the metal guarantees the mechanical stability of the device, whereas the HA coating ensures its biocompatibility. It has also been shown that the presence of HA near ~~a~~ viable bone increases the bonding force [16,17]. In the presence of HA layers, the osteointegration process provides ~~for the~~ a pH decrease at the interface between the coating and tissue, leading to partial dissolution of the HA coating and the subsequent release of Ca^{2+} and HPO_3^{2-} ions. These precipitate into apatite crystals while simultaneously incorporating the collagen matrix. The final result of the bone repair process is the production of osteoblast cells, whose ossification restores the normal mechanical properties of the bone tissue, which is then able to self-repair [18].

Among the many conventional deposition methods of hydroxyapatite coatings, such as plasma spraying [19], electrodeposition [20,21], electrophoretic deposition [5][8,22], sono-electrodeposition [23], sol-gel [24], plasma~~-~~ spraying [19,25,26] and many others [27], in this work we ~~have~~ opted for ~~the~~ galvanic deposition [28][29]. This deposition method does not require an external power supply~~,~~ because it consists ~~in putting~~ of placing two electrodes in galvanic contact ~~two electrodes~~, the substrate (on which the deposition occurs (AISI 304 steel)) and a sacrificial anode (Zn or Al), in an electrochemical cell containing a solution of calcium and phosphate ions. ~~Due only to~~ Because of the difference in the electrochemical redox potential of the galvanic couple and starting from the salts present in the solution, ~~on the cathode~~ the deposition of calcium

phosphate compounds takes place on the cathode. In addition to the possibility of operating without an external power supply, a key advantage of ~~the~~ galvanic deposition is the growth rate control by changing the anodic to cathodic area ratio. From a technological point of view, deposition through galvanic ~~connection~~connections is very attractive because it is easy to ~~be conducted and scaled~~ conduct and scale up. Galvanic deposition is a ~~consolidate~~consolidated and very versatile method~~,~~ ~~it~~that can be used to obtain different materials [30][31][32], even in a nanostructured form [33][34][35][36][37][38][39][40][41][42][43]. ~~Besides~~In addition, this method is cheaper and simpler than the electrodeposition process and ~~it allows to realize~~ allows ~~the realization of~~ for achieving a coating with ~~a~~ good adhesion to the substrate and with the absence of cytotoxicity [28][44].

In this work, ~~the~~ attention ~~was~~ is focused on the deposition of composite coatings of calcium phosphate and polyvinyl acetate (PVAc) achieved via the galvanic deposition method on 304SS. The aim is to obtain a coating that is able to isolate the 304SS substrate from the body fluid to prevent its corrosion. AISI 304 steel (304SS) is a steel used for many applications and is characterized, in comparison to 316L (~~that~~which is ~~the~~ a ~~steel~~ commonly ~~-~~used steel for biomedical applications), by a low cost but also by a low corrosion resistance in the presence of chlorides due to the absence of Mo [46].

PVAc ~~was~~ is preferred because it contributes to ~~minimize~~minimizing the cytotoxicity of the coating, favoring the proliferation of cells and even creating ~~even~~ a new cellular matrix that could guide tissue regeneration [47]. Furthermore, PVAc guarantees the formation of a layer that is very adherent to the metallic substrate (as demonstrated by Hu et al [48][48]). These authors have also shown that HA/PVAc coatings~~,~~ obtained by

co-electrodeposition on a Ti–6Al–4V alloy~~, presents~~ present a high bioactivity, attributable to a remarkable change ~~on~~in the surface morphology of the hybrid bioceramic coating. Abdal-hay et al~~,~~. ~~have~~ also demonstrated that the incorporation of PVAc in the HA coatings provides a significant improvement in the corrosion resistance of titanium ~~substrate,~~substrates due to ~~a~~ the strong chemical interfacial bonding between the substrate and the coating [50]. ~~Besides,~~ In addition, the authors ~~have~~ demonstrated that the biocompatibility of the coated Ti was significantly higher than that of the pure titanium~~-~~ substrates. Finally, Afshar et al.~~, have~~ also ~~proven~~proved that the presence of PVAc in the coatings ~~improve~~improved the crystallization of HA. ~~As a matter of~~ In fact, the XRD (Xray diffraction) ~~patters~~patterns showed ~~the~~an increase ~~of~~in the HA peaks with an ~~the increase of~~ increasing vinyl acetate concentration in the deposition solution [51].

~~At our~~To the best of our knowledge, to date the deposition of HA/PVAc composite coatings ~~HA/PVAc was~~has only been ~~carried out~~ performed ~~only~~ on Ti or its alloys. The aim of this work is to demonstrate that opportunely~~-~~ coated 304SS substrates also exhibit ~~also~~ good corrosion properties without affecting the organism in which they can ~~be~~ potentially be implanted. To prove this, an in~~-~~ vitro characterization campaign was ~~carried out~~performed~~,~~ by immersing the samples in SBF (simulated body fluid) to perform corrosion tests and to quantify the metal ~~ions~~ion release. Moreover, the cell biocompatibility of the coating was investigated through osteoblastic cell cultures to investigate the possible onset of cytotoxicity due to the release of metal ions from the SS substrate.

Experimental Details

The cementation process involves ~~the~~ galvanic contact between two electrodes placed in separate cells. A scheme of the setup used for the deposition of coatings is reported in Figure 1. In the anodic compartment, a sheet of Zn or Al is inserted in a 1 M solution of NaCl, while in the cathodic compartment, an AISI 304 steel sheet is immersed in a solution of $Ca(NO_3)_2 \cdot 4H_2O$ at 0.061 M and ~~of~~ $NH_4H_2PO_4$ at 0.036 M. In the catholyte (50 mL), vinyl acetate (VAc) was added at different ~~concentration~~concentrations (0 mL, 0.75 mL, 1.5 mL), with the aim of incorporating this polymer into the coatings ~~in order~~ to increase its biocompatibility and adhesion to the SS substrate. A fresh solution for each experiment was prepared. The pH of the solution was 4.7 and remained unchanged after the addition of ~~the~~ VAc. As a substrate, commercial 304 SS (UNS S30400, 0.025% wt. C, 18.18% wt. Cr, 8.03% wt. Ni, 1.66% wt. Mn, 0.31% wt. Si, 0.031% wt. P, and 0.001% wt. S, and Fe at balance) sheets (7 × 1.5 × 0.5 cm) were used. Before deposition, the SS was degreased in an ultrasonic bath with pure acetone, mechanically polished with abrasive paper of different grades (#150, #300, #800, #1200) and ultrasonically rinsed in distilled water. Finally, the SS substrate was dried in air at 50°C. After cleaning, the SS surface was delimited with an insulator to expose an area of 1.14 cm^2. Sacrificial anodes of Zn or Al (sheets of 7×3 cm) were employed~~,~~ and cleaned using the same procedure followed for the SS substrate. The anode exposed area was approximately ~~about~~ 27 cm^2. Specific anode consumption was measured by means of gravimetric measurements using a Sartorius microbalance (mod. Premium Microbalance ME36S). The coatings were obtained at different temperatures (25°C and 50°C), deposition times (24 hours and 72 hours) and driving forces (changing the sacrificial anode~~,~~ by using either zinc, with a standard potential of -0.762 V, or aluminum, with standard potential of -1.66 V). The deposition at

50°C ~~were~~was ~~carried out~~conducted by using ~~a~~ heating chambers with natural convection and an uncontrolled internal atmosphere (Binder, mod ED56).

~~Coatings'~~ The morphology of the coatings was investigated using ~~a~~an FEG-ESEM microscope (QUANTA 200)~~,~~ equipped with ~~Energy Disperse Spectroscopy~~an energy dispersive spectroscopy (EDS) probe. The crystallographic structures of the coatings ~~was~~ were investigated by X-ray ~~Diffraction~~diffraction using a RIGAKU instrument (model: D-MAX 25600 HK). Diffractograms were obtained in the 2θ range from 10° to 60° by means of ~~the~~ copper Kα radiation (λ= 1.54 Å) with the following ~~set up~~setup conditions: a tube voltage of 40 kV, a current of 30 mA, a scan speed of 4°/min, and a sampling of 0.01°. Diffraction patterns were analyzed by ~~comparison~~ comparing them with the ICDD database [52]. The Raman spectra were obtained using a Renishaw (inVia Raman Microscope) spectrometer. The excitation was provided by the 532 nm line of a Nd:YAG laser calibrated by the Raman peak of ~~a~~ polycrystalline Si (520 cm^{-1}). The Raman spectra were analyzed ~~by~~ via comparison with the RHUFF database [53]. FT-IR/ATR ~~analysis~~analyses were carried out by using a Perkin-Elmer FT-IR/NIR Spectrum 400 spectrophotometer. The spectra were collected in the range 4000–400 cm^{-1}.

Static contact angles were measured on all samples by using distilled water and an SBF solution as fluids using an FTA 1000 (First Ten Ångstroms, UK) instrument. In particular, 4 µL of fluid were dropped on the sample surface. Images of the drop on the sample surface were taken at a time of 10 s. At least 5 spots of each sample were tested, and the average value was taken. Inductively ~~Coupled Plasma Optical Emission Spectrometry~~coupled plasma optical emission spectrometry (ICP-OES, PerkinElmer Optima 2100 DV) was also performed ~~in order~~ to evaluate the concentration of metal ions released after 21 days of aging

of the samples in SBF at a temperature of 37±1°C. A calibration line was ~~carried out~~determine for each metal ion to detect ~~(~~Fe, Ni, Cr, Ca, and P~~)~~ by using standard calibration solutions. All characterization methods have been detailed in our previous works [44] [54] [55] [56].

The corrosion tests were ~~carried out~~conducted by immersing the samples in an SBF solution, prepared according to the procedure reported in [10], for a period of 21 days at a temperature of 37°C. In particular, the ~~measurements of~~ OCP (open circuit potential)~~,~~ and polarization measurements (from which the Tafel curves were obtained) were adopted to evaluate the potential and corrosion current density. In ~~details~~detail, each sample was immersed in an SBF solution (aging solution) and periodically~~,~~ (at the day scale)~~,~~ ~~it was~~ extracted and rapidly transferred into a fresh SBF solution to ~~carried out~~conduct electrochemical tests. At the end of these experiments, the sample was transferred again into the aging solution, ~~where~~which remained for some days ~~up to~~ until the successive electrochemical tests. To stabilize the interface conditions, it was ~~chosen~~ decided to wait half an hour before recording the OCP values [28]. The ~~P~~polarization measurements were performed with a scan rate of 5 mV/sec in a potential range of ±150 mV with respect to the OCP value. The samples were also analyzed using impedance measurements at OCP in the frequency range from 0.1 Hz to 100 kHz, with 0.010 V of AC perturbation. ~~The~~ ZSimpWin software was used for the fitting, and, for comparison, ~~also~~ the SS substrate was also characterized. ~~Conventional~~ A conventional three-electrode cell with a platinum wire as the counter electrode and a 3.0 M Ag/AgCl as the reference electrode was used.

~~As regards~~ For the cytotoxicity tests, uncoated and coated samples were cut into rectangles of 3×1.5 cm, rinsed with ~~milli~~Milli-Q water, immersed in ethanol for 24 hours and

then sterilized in an autoclave at 121°C under a high pressure. Each sample was then incubated with Dulbecco's Modified Eagle Medium (DMEM, Sigma Aldrich) at 37°C for 24 hours with a volume/surface ratio of 5 mL/cm^2 [56]. Afterwards, the as-treated media were collected in a 50 mL falcon and utilized for the cytotoxicity test. MC3T3-E1 pre-osteoblastic cells purchased from Sigma-Aldrich (ECACC) were cultured in DMEM ~~added~~supplemented with 10% fetal bovine serum, 1% glutamine and 1% antibiotic at 37°C and in a 5% CO_2 atmosphere. A total of 10^4 osteoblastic cells were seeded into the wells of a 24-well culture plate (10 mm diameter) and incubated with normal DMEM at 37°C and 5% CO_2. After 24 hours, the medium was replaced with the treated media. For comparison, normal DMEM was used as a positive control to evaluate the effect of coatings on the SS substrate, whereas DMEM treated with naked stainless steel was used as a negative control. Cytotoxicity assays were ~~carried out~~conducted after 0, 2, 5 and 7 days of culture. The ~~C~~cell viability was assessed with CCK-8 (Cell Counting Kit-8, Sigma-Aldrich), utilizing the highly water-soluble salt WST-8 that, in the presence of living cells, produces a water-soluble formazan dye, giving a yellow color detectable at 450 nm. The obtained data were compared using ~~the~~ Student's t-test. A P value < 0.05 was considered significant.

Each experiment reported in this work was repeated at least three times.

Results

While the galvanic deposition of ~~Brushite~~brushite (BS) and HA has previously been demonstrated by us, the deposition of ~~the~~ PVAc ~~to date~~ has to date only been obtained ~~only~~ by electrodeposition. Consequently, to demonstrate that this polymer can also be electropolymerized through the galvanic method, initial experiments were conducted using

~~exactly~~ the exact same scheme reported in Figure 1 but using ~~in the cathode side~~ a solution containing only the vinyl acetate monomer on the cathode side. In particular, ~~the~~a concentration of 1.5 mL was tested, and ~~the~~ deposition was ~~carried out~~performed for 24 hours and 72 hous at 25°C, keeping all the other parameters unchanged (SS area, anode area, anodic solution, initial treatments). To verify the formation of the PVAc deposit, the samples were analyzed ~~by~~ via SEM and EDS (Figure 1S shows these results). In particular, as ~~it was to be~~ expected, due to the low concentration of the monomer, the polymer formed in small areas of the electrode that tended to increase with the deposition time. ~~As a matter of~~ In fact, the presence of carbon and oxygen and the elements of the substrate ~~was~~ were detected via EDS. Being of an organic nature, this deposit tends to degrade under ~~the~~ an electron beam. These results therefore confirm the possibility of obtaining the electro-polymerization of the PVAc by means of galvanic deposition according to the mechanism proposed by Samide et al. [58].

In Figure 2 ~~the~~, SEM images of BS/HA/PVAc coatings obtained at different temperatures (25°C and 50°C) and VAc concentrations (0 mL, 0.75 mL, 1.5 mL) are shown. In particular, the top- views reported in Figure 2 (Figure 2S for zinc anode) show the typical needle-shaped form of the calcium phosphate-based layers. Although a complete covering of the metal substrate could be observed in each sample, the morphologies are dissimilar among them. ~~Basically~~Essentially, galvanic coupling with the Al anode (Figure 2a) leads to coatings consisting of needles with higher ~~dimension respect to~~dimensions than galvanic coupling with the Zn anode~~, thanks~~ due to a more favorable driving force. For both sacrificial anodes, upon increasing the temperature (Figure 2d), the morphology appears to be more disordered, probably due to a more massive deposition ~~owing to~~ from the~~a~~ more favorable kinetics. In the presence of polymers, coatings are constituted by agglomerates of a smaller size than those of

just BS/HA ~~only~~ (~~(~~Figure 2b-c), ~~in particular~~ particularly at a high temperature (Figure 2e-f)).

~~Sample~~Samples were also characterized ~~by~~ via EDS (Figure 4S), from which the Ca/Fe (this value permits ~~to qualitatively estimate~~qualitative estimation of the thickness of the deposit) and Ca/P (this value permits ~~to estimate~~estimation of the chemical composition of the deposit) ratios were calculated and reported in Table I for the aluminum anode (Table 1~~I~~S is for the zinc anode). In particular, the EDS analyses were performed in different areas of the samples, and in the tables the average value is reported. With ~~the~~ an increase in the deposition time and temperature, a corresponding increase ~~of~~in the Ca/Fe and Ca/P ratios can be observed. In particular, the values of the latter are~~,~~ above 1.4 in all deposition conditions ~~(above 1.4)~~ and increase with the deposition time and temperature up to ~~about~~approximately 1.7.~~.~~ ~~T~~thus~~,~~ suggesting a more significant HA formation.

Figure 3 (Figure 5S for zinc anode) shows the diffraction patterns of the coatings obtained ~~at~~under different conditions. The diffraction peaks of HA and BS were identified through comparisons with the ICDD database [52] (card ~~number~~numbers 72–0713 for ~~Brushite~~brushite and 72–1243 for ~~Hydroxyapatite~~hydroxyapatite). The diffraction pattern of 304SS was also reported ~~in order~~ to highlight the ~~peaks~~peak shielding due to the presence of coatings. Figure 3a shows that in the samples obtained after 72 ~~72h~~hours of galvanic deposition, where it is possible to identify more peaks related to BS with respect to HA~~,~~ when ~~comparing~~compared to the sample abstained after 24 h. In Figure 3b, for galvanic deposition ~~carried out~~performed at 50°C, the HA peaks are more easily identifiable than the BS ~~ones. As regards deposit~~ peaks. Regarding deposits obtained ~~by~~ via galvanic coupling with Zn, the XRD patterns (Figure 5S) reveal that the coatings were constituted by a mixture of HA/BS. Once again, typical HA diffraction peaks are more detectable than BS ~~ones~~ diffraction peaks

for samples obtained at 50°C (Figure 5S-b).

A ~~L~~localized micro-Raman analysis was executed ~~in order~~ to further scrutinize the deposit phase composition. As shown in Figure 4, both the HA and BS phases were found and identified ~~by~~ via comparison with the RUFF database [53]. In agreement with the XRD results, the Raman spectra showed that BS peaks are more abundant and sharper than the HA ~~ones~~peaks. The presence of PVAc was identified through the peaks at 900 cm^{-1} (C-C stretching) and 1135 cm^{-1} (C-O stretching), even if it was difficult to detect in all investigated areas via micro-Raman ~~the presence of PVAc,~~ due to its low content [59] and ~~to~~ the proximity of the BS and HA Raman modes. The main mode at ~~about~~approximately 2930 cm^{-1} (C-H stretching) was not observed. In the case of the zinc anode, very similar results were attained (Figure 6S).

Samples were also characterized ~~also~~ after 21 days of aging in the SBF solution, ~~and~~ with the results ~~are resumed~~shown in Figure 5. It is interesting to note that after aging, the BS peaks are no ~~more~~longer detectable, and the mode of vibrational stretching of ~~the~~ PVAc is visible at ~~about~~approximately 2930 cm^{-1}, thus confirming the presence of the polymer. The low height and the wide broadness of this peak confirm the initial amorphous nature of the polymer. After aging in SBF, the EDS spectra (Figure 10S) reveal that all samples tend to have a Ca/P ratio of ~~about 2. Coating~~approximately 2. The coating morphology, after immersion in SBF~~,~~ (Figure 5a~~,~~), is quite similar (Figure 9S) for all samples, despite the variation ~~of~~in the deposition parameters, such as the time and amount of monomer inserted in the deposition solution.

To further verify the presence of PVAc, the FT-IR/ATR spectra were also recorded. The FT-IR/ATR spectra of coatings before and after aging in SBF are ~~showed~~shown in Figure 6a, while the infrared band positions and their assignments are summarized in Table ~~S~~5S.

Brushite formation was confirmed ~~by~~ via the FT-IR/ATR spectra before aging in SBF, as the characteristic BS peaks ~~of BS show up~~appeared [59,60]. In the same samples, it is difficult to appreciate the presence of HA, as the majority of its peaks ~~are overlapped by~~ overlap with the more intense BS ~~ones~~peaks. Before aging in SBF, the samples containing PVAc are mainly characterized by ~~the~~ very intense BS peaks, ~~though~~although the peaks attributable to the PVAc phase are well distinguishable. In particular, two peaks at 2928 cm^{-1} and 2854 cm^{-1} can be noticed, which can be assigned to the CH_2 symmetric and asymmetric stretching ~~vibration~~vibrations of PVAc, respectively. The C=O vibration of the polymeric phase was detected through the peak at 1722 cm^{-1}. The peaks at 1434 cm^{-1} and 1376 cm^{-1} can be ascribed to ~~the~~the δ(CH_2) and δ(CH_3) ~~vibration~~vibrations of PVAc, respectively, while the peak at 1238 cm^{-1} is assignable to the C-O stretching (asym) of PVAc [62,63]. Other characteristic peaks of PVAc, such as C-C-C and C-C-O at 1121 cm^{-1} and the C-C group vibration at 1025 cm^{-1}, are covered by the more intense BS signal ~~of BS~~.

The formation of HA after aging in SBF was confirmed by FT-IR/ATR (Figure 6a, Table ~~S5~~5S), which indicated the loss of the typical brushite peaks associated with the stretching frequencies (νOH: 3540–3153 cm^{-1}) and bend mode (δOH: 1642 cm^{-1}), ~~and~~ as well as the presence of the characteristic peaks of HA [60]. Again, the samples containing PVAc showed the ~~above discussed~~ abovementioned characteristic peaks ~~of PVAc also~~ after ~~the~~ aging in SBF. In this case, the peaks attributable to PVAc are less intense than those observed in ~~pre-aging~~preaging coatings. This is presumably related to a partial loss of the polymer phase during aging in SBF~~,~~ due to HA formation.

The contact angle value, which is an indicator of the surface wettability and biocompatibility, was determined by the static contact angle of distilled water and SBF

solution on coating surfaces before and after aging in SBF. Before aging, all samples, regardless of the polymer content, exhibit a very low contact angle both in water and in SBF (Figure S77S). After aging, the behavior tends to become different~~,~~ (Figure 6b, ~~(~~see also Figure S88S). By comparing the HA 1D and HA 3D coatings, it can be noticed that both the water and SBF contact ~~angle~~angles decreased upon increasing the deposition time. This result can likely be ~~likely~~ ascribed to the roughness and the change ~~of~~in grain size of the coatings occurring upon increasing the deposition time. In particular, it was demonstrated that the contact angle on HA decreases upon decreasing the HA grain size because of an increase ~~of~~in the specific surface area [64,65]. This evidence is in line with the XRD results shown above for the sample obtained at 50°C, i.e., a decrease ~~of~~in grain size with an ~~the increase of~~ increasing deposition time. Coherently, the SEM images of HA 1D and HA 3D (Figure S99S) indicate that the latter is characterized by a slightly higher roughness due to the presence of a smaller grain size. As expected, both the HA/PVAc 1D and 3D coatings display a sharp decrease ~~of~~in the contact angles of water and SBF ~~if~~ when compared to the HA coatings. More ~~in detail~~specifically, the mean contact angles of HA/PVAc 1D are 11.5° and 11.9° for water and SBF, respectively, while they are lower than 10° for both ~~the~~ fluids in contact with HA/PVAc 3D. Since the roughness of the samples ~~are~~is very similar to that of HA coatings (Figure S99S), this result can be ascribed to the presence of ~~the~~ hydrophilic PVAc.

Electrochemical corrosion tests (open circuit potential monitoring (OCP), potentiodynamic polarization and impedance spectroscopy) were ~~carried out~~conducted in vitro using ~~a~~ an SBF solution at 37°C~~, in order~~ to assess the performances of the protective layers. The analysis of the OCP (Figure 11S) is very useful, as abrupt changes in the OCP are the consequence of damage to the coatings.~~,~~ ~~which~~ This could be caused by the continuous

evolution of the coating, which in contact with the SBF is partially solubilized and redeposited. Already after a day of immersion, the OCP value is approximately constant during the 30 minutes of monitoring (the deposit is therefore stable), and between the different days of being monitored, there is only a small variation in the values, due to the continuous process of dissolution and reprecipitation that occurs in SBF [28].

Figure 7a shows Tafel plots for the coatings deposited by Al coupling at 25°C with 1.5 mL of VAc (see also Figure 12S). It was reported also uncoated 304SS The corrosion behavior of uncoated 304SS was also reported in order to compare the improvements provided by coatings. The behavior of SS is similar to that reported in [45]. For coated samples, the continuous variation of Tafel plots, as reported in [66,67], is due to the continuous dynamic process of BS/HA coatings in the SBF solution that involves dissolution, precipitation and ion exchange, leading to the changes in the composition, morphology and thickness, as discussed above discussed. The corrosion potential (E_{corr}) and corrosion current density (i_{corr}) were calculated by extrapolation of the Tafel's curve, and the results are listed in Table II (see also Table 6S).

Bode and Nyquist plots after different timetimes of aging in SBF are showedshown in Figures 8 (a-f), for coatings grown at 50°C with 1.5 mL of vinyl acetate and for 72h72 h. The Iimpedance spectra were fitted through the use of an equivalent circuit (EC). In particular, for this sample, the best fitting was obtained by using the equivalent circuit R(CPE(R(CPE(RW)) (Figure 13S, Table –7S) leading to a low Chichi-square (almost inon the order of 10^{-4}). For each parameter, the relative error was less than 10%.

Moreover, it should be noted that in some cases, at different aging timetimes, a superior best fitting was obtained by using the equivalent circuit R(CPER)(CPE(RW)). This behavior,

according to [66], is attributable to the dynamic balance of dissolution/reprecipitation, to which the coatings of calcium phosphate are subjected to when immersed in SBF.

CoatingThe coating anticorrosion action was also scrutinized by the quantification of the release of the metal ions from the SS substrate in the SBF solution. In particular, the concentrationconcentrations of Fe, Ni and Cr ions in the SBF (after 21 days) waswere measured. Ions The ion concentration was evaluated by ICP-OES after construction of the relative calibration line for each element. For comparison, also the as-prepared SBF was also analyzed. Ca- and P- ions concentration was -ion concentrations were also evaluated in order to confirm the progressive conversion of the coatings. ResultsThe results of these tests, for samples after 24 hours and 72 hours of galvanic deposition couplingcoupled with the Al anode without and with 1.5 mL of VAc, are reported in Table III. Very low values of metal ions were found, while, with respect to the as-prepared SBF, lower and higher concentrations of Ca and P were measured, respectively.

The cytotoxicity of HA/BS/PVAc composite coatings prepared under different conditions was tested in- vitro tested by using preosteoblastic cells. Cell cultures were carried out performed using the media incubated for 24 hours with the different samples at an established volume/surface ratio. Specifically, the cytotoxicity tests were carried outconducted on the samples obtained with an aluminum anode at room temperature, with a deposition timetimes of 24 and 72 hours, with and without 1.5 mL of VAc. Cell viability was verified for 7 days of culture. The results of these tests are shown in Figure 8. After 2 days of culture, no statistically significant difference between the absorbance values present in the controls and in the samples werewas detected. At day 5, identical absorbance values were recorded for the control and the samples BS/HA and BS/HA/PVAc samples obtained after 24 hours of

deposition, whereas slightly lower values were observed for the ~~samples~~ BS/HA and BS/HA/PVAc samples realized after 72 hours of deposition. However, at this ~~time~~ point in time, the absorbance values of ~~absorbance of~~ cells grown ~~with~~in normal and coated ~~treated~~ media ~~are~~were higher ~~with respect to the values~~ than those of cells grown in the medium treated with naked metal (negative control). At day 7, the absorbance values of treated samples are ~~about~~approximately threefold with respect to the negative control, whereas they ~~result to be~~ are lower with respect to the positive control in a range spanning from 82 to 90%. It is, however, important to ~~underline~~emphasize that in all cases, the viability of the cells grown with the incubated media~~,~~ was abundantly over 70% with respect to the control, thus confirming the non-cytotoxicity of the tested materials, according to the ~~followed~~following ISO standard [68].

Overall, it is possible to state that, with regard to the culture period taken under consideration, the presence of coating eradicates the basal cytotoxic effect given by pristine stainless steel~~,~~ without secondary effects on ~~the~~ physiological cell growth.

Discussion

Following the deposition mechanism proposed in [29] and the ~~scheme of~~ galvanic cell scheme reported in Figure 1, after ~~the~~ immersion of the anode (Zn or Al) in the ~~NaCl~~ 1 M NaCl solution ~~the~~, subsequent oxidation reactions occur (depending on the sacrificial anode used):

$$1) \quad Zn \rightarrow Zn^{2+} + 2e^- \quad (E^0 = -0.76\,V/NHE)$$

$$2) \quad Al \rightarrow Al^{3+} + 3e^- \quad (E^0 = -1.66\,V/NHE)$$

The electrons produced at the anode flow through the external connection and reach the surface of AISI 304, where ~~reduce the nitrate ions~~nitrate ions are reduced according to the following cathodic reaction [69]:

3) $NO_3^- + H_2O + 2e^- \rightarrow NO_2^- + 2OH^- \quad (E^0 = 0.0835 - 0.059pH\ V/NHE)$

In addition, the cathodic production of OH^- ions also comes from the reduction of water and oxygen, following the reactions

4) $2H_2O + 2e^- \rightarrow H_2 + 2OH^- \quad (E^0 = 0.00 - 0.059pH\ V/NHE)$

5) $O_2 + 2H_2O + 4e^- \rightarrow 4OH^- \quad (E^0 = 1.23 - 0.059pH\ V/NHE)$

The cathodic generation of OH^- ions causes a local increase ~~of~~in the pH at the electrode/electrolyte interface. The pH increase displaces the dissociation balance of di-hydrogen phosphate ions ($H_2PO_4^-$) in favor of hydrogen phosphate ions (HPO_4^{2-}), ~~that~~which occurs above pH 7.2~~ pH value~~. On the substrate surface, ~~T~~the formation of HPO_4^{2-} ions leads~~, on the substrate surface,~~ to deposition of BS according to the reaction

6) $Ca^{2+} + HPO_4^{2-} + 2H_2O \rightarrow CaHPO_4 \cdot 2H_2O \downarrow$

Since a porous BS deposit is formed, the cathodic reactions might not be ~~not~~ inhibited, causing a further increase in pH. ~~When a~~A pH value of ~~about~~approximately 12 ~~is reached, this~~ is ~~possible~~ only possible thanks to nitrate reduction [69], and hydrogen phosphate dissociates

in orthophosphate (PO_4^{3-}), leading to HA precipitation according to the reaction [70]

$$7) \quad 10Ca^{2+} + 6PO_4^{3-} + 2OH^- \rightarrow Ca_{10}(PO_4)_6(OH)_2 \downarrow$$

In the presence of the VAc monomer, ~~also the~~ co-deposition of PVAc also occurs throughout the radical polymerization of VAc following the mechanism proposed by Samide et al. [58]. Radical polymerization is a three-stage ~~processes~~process: initiation, propagation, and interruption. In our case, the initiation stage of electropolymerization, during which free radicals are formed, was induced by the reduction reaction of the monomer protonated molecules adsorbed on the cathode.

$$8) \quad (VAc - H^+)_{ads} + e^- \rightarrow (HVAc^{\cdot})_{ads}$$

These radicals activate other adsorbed monomer molecules with the consequent formation of ~~macro-radicals~~macroradicals, following the reaction

$$9) \quad (HVAc^{\cdot})_{ads} + (VAc)_{ads} \rightarrow (HVAc - VAc^{\cdot})_{ads}$$

During the propagation step ~~the~~ radical chain reactions occur, followed by recombination and disproportionation of ~~macro-radicals~~macroradicals to form PVAc.

The global process leads to the deposition of composite coatings made of BS, HA and PVAc, and is only due to the difference in the standard electrochemical potential between steel and the less noble anode. ~~Thin~~The thin difference ~~on~~in redox potentials provides the driving force for the electrogeneration of ~~base,~~bases necessary to precipitate BS and HA~~,~~ and

~~radicals~~radical formation, which is indispensable to the initiation step of the radical polymerization of PVAc.

The morphology of coatings is strictly ~~depended~~dependent on the temperature of the galvanic deposition and the type of anode. ~~On the contrary~~In contrast, morphology is independent of the deposition time. The type of anode establishes the driving force of the galvanic processes due to its redox potential. ~~The galvanic~~ Galvanic coupling with the Al anode has ~~the~~a higher driving force~~, (about 1V~~ (approximately 1 V higher than that with Zn), and in this case (Figure 2a), the coating consists of needles with higher ~~dimension respect to~~ dimensions than Zn. As expected, the temperature plays a key role in the sample morphology~~,~~ since the kinetic corrosion of the anode increases with an ~~the increase of~~increasing temperature. With an ~~the increase of~~increasing anode corrosion, the generation rate of OH^- ions increases. The effect of increasing ~~of~~ the OH^- concentration consists ~~in~~of a massive deposition with the ~~consequently~~consequent formation of a more disordered morphology that is ~~clear~~clearly visible in Figure 2d, relative to the samples obtained at 50°C. The disordered morphology can be ~~attributable~~ attributed to the high deposition rate at 50°C. In particular, at 50°C the higher deposition ~~kinetic favors~~kinetics favor the nucleation of the grains of the calcium phosphate-based compound and their massive deposition. ~~While at~~ At 25°C, the slower deposition rate favors the growth of the grains. Thus, it is reasonable to expect the formation of deposits with different ~~microstructure~~microstructures as the temperature changes, which could affect their performance. In Table 2S, the specific anode consumption was reported. It is important to ~~underline~~emphasize that, although these data are coherent, because an increase ~~of~~in anode dissolution was measured with time and temperature, they are not ~~to be~~ considered ~~as~~ absolute values. In fact, although we have operated in separate cells,

precipitation of oxides/hydroxides at the anode surface occurs. The presence of these precipitates influences the value of the final weight of the anode. For this reason, a new anode was used for each experiment.

~~By~~ Via SEM, it was not possible to detect the presence of PVAc because it is reasonable to think that the polymer is intimately incorporated in the HA/BS deposit. However, the addition of the polymer leads to the formation of a more homogeneous and uniform deposit, especially in the case of coatings obtained using aluminum as the anode. In particular, the presence of the polymer leads to the formation of clusters of ~~deposit~~deposits that are much more similar to ~~each~~ one another than those obtained without the polymer. An interesting aspect of the BS/HA/PVAc composite coatings is that they are extremely adherent to the steel substrate. This was qualitatively verified by simple peeling- tape- tests [71] and by resistance to prolonged exposure to ethanol ultrasound baths, unlike ~~the~~ polymer-free deposits, which instead tend to come off very easily. This result is coherent with the literature data [48][48][50] and is imputable to the presence of polymer.

~~As regards~~ Regarding the deposition time, ~~it was not observed any~~ no particular change in sample morphologies (for both sacrificial anodes)~~–~~ was observed because this deposition parameter ~~affects~~ only affects the thickness of the coatings (Figure 3S), as confirmed ~~by~~ via EDS analysis (Table I). In particular, ~~the~~ qualitative information about the thickness of coatings comes from the Ca/Fe ratio, while ~~from Ca/P values~~ the chemical composition can be evaluated from the Ca/P values, taking ~~into account~~ the stoichiometric ratio for BS (Ca/P=1) and HA (Ca/P=1.667) into account [72]. The presence of the monomer in the solution does not influence the composition of the deposit, while a change can be observed with the deposition times and temperatures. As a matter of fact, as the Ca/Fe ratio rises with both

parameters, it is plausible to suppose that the thickness of the coatings increases accordingly. As far as the chemical composition is concerned, the Ca/P ratio value, which in all deposition conditions always remains ~~always~~ above 1.4, suggests that a mixture of BS and HA was produced. The observed increase ~~of~~in this ratio up to 1.7 with the deposition time and temperature~~,~~ seems to indicate a parallel increment of the HA amount with respect to BS~~,~~ due to the growth of the interfacial pH ensured by long deposition times and high temperatures. Finally, ~~as regards~~regarding galvanic coupling with Zn, both the Ca/Fe and Ca/P ratios are higher than those obtained ~~in~~under the same conditions but using aluminum; moreover, in some cases~~,~~ the ~~peak of~~ Fe peak was not visible, thus revealing the presence of ~~a~~ a very thick coating. This is attributable to the different behaviors of the two sacrificial anodes with respect to pH [73]. In particular, although ~~the~~ deposition was ~~carried out~~conducted in a two-compartment cell, a slight pH increase was also observed ~~also in~~ on the anodic side. In the case of aluminum, a pH above 4 leads to the formation of a layer of $Al(OH)_3$ that could slow down the galvanic process. ~~Reversely~~Conversely, for zinc~~,~~ the slight increase in the pH of the anodic solution does not change its activity.

PVAc was not identified though the XRD analysis, probably due to its very low content and/or its amorphous nature, as reported by Abdelghany et al. [63]. On the other hand, the XRD analysis confirms (Figure 3) that the layers were almost made up of a BS/HA mixture, according to the results obtained in [29]. The presence of the HA/BS mixtures probably stems from the short precipitation times, which do not allow for the formation of HA alone.

Upon increasing ~~of~~the deposition time, the BS diffraction peaks tend to dominate with respect to those of HA, ~~owing~~ due to the progressive deactivation of Al related to the formation of $Al(OH)_3$ that slows ~~down~~the cementation process (and thus the continuous

increase ~~of~~in the interfacial pH). According to Nur et al. [74], if the interfacial pH ~~was~~is not maintained at a value above 12, a reversible reaction between HA and BS occurs.

$$10)\ 10CaHPO_4 + 2OH^- \leftrightarrow Ca_{10}(PO_4)_6(OH)_2 + 4PO_4^{3-} + 10H^+$$

~~On the contrary~~In contrast, with an ~~the increase of~~ increasing temperature, thanks to the high rate of anode corrosion, the relative amount of HA ~~augments~~increased, as outlined by the diffraction peak intensification. We ~~have~~ evaluated the grain size by using Sherrer's equation [75], focusing on the BS peak located at ~~about~~approximately 11°, present in all spectra (Table~~.~~ ~~S4~~4S). At 25°C, the deposit grain size increases with the deposition time~~,~~ due to the gradual growth of the nucleation sites, whereas the presence of ~~the~~ polymers~~, for both anodes,~~ has little influence for both anodes. One could therefore conclude that at 25°C, as the deposition time ~~goes up~~increases, the growth of existing grains prevails over the nucleation of new grains.

On the other hand, the effect of temperature is very remarkable, and in particular, at 50°C the average grain size is much smaller and tends to decrease with the deposition time. This is attributable to the increased concentration of OH^- determining a parallel significant precipitation of small grains, whose growth is hindered by the deposition of new grains. We could therefore conclude that at 50 °C, as the deposition time progresses, the nucleation of new grains prevails over the growth of existing grains. In the case of the aluminum anode, for both temperatures~~,~~ relatively smaller grains are obtained due to the greater driving force tending to favor nucleation. However, for both anodes~~,~~ the effect of a temperature rise is to diminish the crystallinity of the coatings. In particular, the poor crystallinity at 50°C was a

remarkable result, and a low crystallinity should ensure a slow dissolution rate into the SBF solution, thus permitting an adequate time for the growth of new natural tissue inside the coating pores [76].

Thus, it can be summarized that long deposition times favor the formation of BS with respect to HA, while an opposite effect can be obtained with an increasing temperature ~~increase~~. This conclusion is also supported ~~also by~~ via micro-Raman spectroscopy ~~that~~, which shows that~~,~~ at a low temperature and for long deposition times, BS is the main compound present in the coatings. Due to the localized nature of ~~this~~these tests, micro-Raman also reveals ~~also,~~the presence of PVAc in some areas of the samples~~, the presence of PVAc,~~ which was also confirmed by the FT-IR-ATR spectra.

It is relevant to ~~underline~~emphasize that the presence of BS in the coatings does not represent a serious problem, as it is easily convertible into HA through ~~a~~ simple immersion in SBF (as reported by Gibson et al. [77] and ~~also~~ demonstrated by us in a previous article [28]). In fact, equilibrium reactions were established during aging in SBF for 21 days, completely converting BS ~~totally~~ in the pure HA phase. This evidence was also confirmed for the coatings obtained in this work, where~~,~~ after 21 days of aging ~~is~~ in the SBF solution, due to the occurrence of dissolution/precipitation reactions (10), the total conversion of BS in HA was revealed. In particular, after aging all investigated samples exhibit a similar morphology (Figure ~~S9~~9S) and similar ~~values of~~ Ca/P ratios (~~about~~ approximately 2), highlighting that all samples tend to have the same composition. ~~As a matter of fact, according~~According to Wei et al. [78], the value of Ca/P after aging close to 2 is attributable to the presence of additional Ca coming from SBF. ~~Besides~~In addition, the EDS reveals the presence of additional elements (Mg, Na, Cl, K, Figure ~~S10~~10S) imputable to the precipitation of chloride salts

and/or other compounds, such as chlorapatite~~,~~ and magnesium phosphate hydrate due to incorporation from SBF solution [28]. Thus, it can be concluded that SBF homogenizes the coatings in terms of the morphology and composition. After aging in SBF, both Raman and FT-IR/ATR ~~show~~showed the presence of PVAc in the coatings. The low intensity of the HA peaks in XRD, Raman and FT-IR/ATR suggests that during conversion in SBF, ~~a~~an HA coating with a low crystallinity is formed. Due to the change in morphology and ~~to~~ the presence of PVAc, the aged HA/PVAc coatings present a very low wettability due to the decrease ~~of~~in the grain size and ~~to~~ the hydrophobicity of PVAc.

The change in composition and morphology of the coatings during ~~the~~ aging in SBF can be followed by ~~the~~ electrochemical in- vitro characterization. In fact, all experimental methodologies (open circuit potential monitoring (OCP), potentiodynamic polarization and electrochemical impedance spectroscopy) showed a continuous evolution of the coating~~,~~ when partially solubilized and redeposited in contact with the SBF ~~is~~. From OCP, we can conclude that coatings play a protective effect, considering that they cause a potential variation towards more noble values with respect to those measured on the uncoated steel substrate. This was also confirmed by Tafel plots~~,~~ (Figure 7a), where the corrosion potential values (E_{corr}) of the samples lay above the E_{corr} of uncoated SS. The ~~C~~coated samples were characterized by more noble potentials starting from the first day of aging, and, in particular, the E_{corr} value after 21 days of aging was approximately 200 mV higher ~~respect to~~than that of uncoated 304SS. These results attest to a satisfying protective quality of the coatings, ~~considering~~ also considering the values of the corrosion current density, which is lower than un-coated steel (even if ~~of~~ on the same order of magnitude). ~~Besides~~ In addition, it is clear that the presence of PVAc (Table 2S) does not affect the anticorrosion features of the coatings, probably due to

its low content. ~~As regards~~ Regarding i_{corr}, the extrapolated values reported in Table ~~2~~ II are affected by fluctuations due to the dissolution precipitation process that occurs in the SBF solution. In particular, as we have demonstrated in a previous work [28], this mechanism is also active ~~also~~ after the complete conversion of BS into HA, as it is related to the equilibrium composition at the coating/SBF interface. The consequence of this continuous dynamic process is that the thickness of the coatings ranges between a minimum and a maximum value [66,79,80], depending on the extent of the dissolution-precipitation, leading to a ~~parallel~~ different parallel corrosion resistance during the aging processes.

Coatings obtained at 50°C, Figure 7b and Table ~~2~~II, showed a ~~slight~~slightly lower corrosion current density and thus a ~~slight~~slightly superior behavior with respect to those at 25°C, due to the formation of a thicker coating covering the SS surface and working as a physical barrier between the SS surface and SBF, as underlined by the corrosion potential that is always positive and higher than uncoated SS for all days of aging. This enhanced performance could also be ~~also~~ attributed to the smallest grain size of the coatings obtained at 50°C using aluminum ~~as~~ as the anode. As reported in the literature, ~~a~~the low crystallinity of the coatings is also an indication of ~~its~~their lower dissolution rate in SBF: the lower the dissolution rate, the greater the protective property of the coatings with respect to the substrate. Furthermore, the lower dissolution rate of this type of ~~coatings~~coating plays its effect, especially in the initial aging phase in SBF, as shown in Figure 7, where the samples with coatings obtained at 50°C~~,~~ after 7 days of aging~~,~~ show a higher corrosion potential than those obtained at 25°C, indicating that the thickness of the coating is larger, thus providing better barrier properties. As the aging time increases, the initial microstructure of the coatings has less ~~and less~~ of an influence~~,~~ because the mechanisms of dissolution and reprecipitation in

SBF ~~taking place~~ tend to make them similar.

The barrier properties of the coatings were also confirmed by ~~the quantification of~~ quantifying the release of ~~the~~ metal ions from the SS substrate in the SBF solution. The measured concentration of metal ions is very low (few ppm for Ni~~,~~ and Cr~~, about~~ and approximately 20 ppm for Fe)~~,~~ and is imputable to the action of coatings that act as a physical barrier against the corrosion of stainless steel. This is a worthy result because, as reported in [81], these low ~~values of~~ metal ion ~~concentration result~~concentrations are harmless ~~for~~ to the human body. ~~As concern~~Regarding Ca and P, it can be observed that after 21 days, the Ca ~~ions~~ion concentration is lower than that in the as-prepared SBF solution~~,~~ due to the incorporation of Ca ions during aging [67]. On the other hand, the P ~~ions~~ion concentration increases after aging with respect to the SBF solution, as phosphate ions are released during the equilibrium reaction between BS and HA (as reported by Nur et al. [74], reaction 10).

The impedance measurements are substantially in accordance with the polarization curves discussed above. The impedance measurements shown in Figure 8 refer to the test after 0, 7 and 21 days of aging. ~~Consistently~~Consistent with the polarization curves, the trends are very similar, and, from the Tafel, we ~~have~~ extrapolated similar values of E_{corr} and i_{corr}. The best fitting is obtained using the circuit proposed in [82] (Figure 10S), corresponding to the inhomogeneous layer model developed by Jüttner et al. [83] used to describe the behavior of defective coatings. In particular, R_s is the solution resistance, CPE_1 and R_1 simulate the behavior of the external porous layer in contact with SBF solution, while CPE_2 and R_2 simulate the behavior of the film in contact with the SS substrate. The Warburg (W) impedance models the diffusion process occurring within the pores~~,~~ due to progressive BS conversion into HA and the incorporation of some species (Figure ~~S1~~10S)~~,~~ present in the

Formatted: Highlight

Formatted: Highlight

Formatted: Highlight

Formatted: Highlight

Formatted: Highlight

SBF solution. The use of CPE reveals ~~a non ideal~~the nonideal capacitor behavior of the coatings [83]. As reported in [84,85], CPE is attributable to various causes (such as the surface roughness and heterogeneities, porosity, and variation of coating composition), which could all simultaneously be present in the case of the coatings obtained in this work. As evident in Table ~~S7~~7S, the values of the fitting parameters change with the immersion time~~,~~ due to morphological and chemical modification of the coatings occurring in the SBF solution. It is thus conceivable to highlight that the layer close to the SS interface has a better quality of the passive layer formed on the SS304 substrate during ~~the~~ immersion in SBF [46]. In fact, the R2 values ~~of R_2~~ are one order of magnitude higher than those related to the SS substrate. However, the ~~values of~~ n_2 values are lower than ~~the~~those of bare steel, confirming that the coatings exhibit a more complex morphology than a simple passive film. In any case, after 21 days~~,~~ the overall impedance is quite similar on all the samples (higher than 10^5 Ohm), confirming that aging in SBF makes the sample morphology very similar.

Formatted: Highlight
Formatted: Highlight
Formatted: Highlight
Formatted: Highlight
Formatted: Highlight
Formatted: Highlight

The good anticorrosion properties of the coatings are accompanied by ~~a~~ non-cytotoxicity, confirmed by *in vitro* test with pre-osteoblastic cells. In fact, the viability of the cells grown with the incubated media was abundantly over ~~the~~ 70% with respect to the control, thus indicating the absence of cytotoxicity, which can also be ~~also~~ related to the very low content of metal ions released in the SBF solution from SS substrate (see ICP-OES).

All the aforementioned results suggest that 304SS coated with calcium phosphate compound and PVAc can ~~be potentially~~ potentially be used for orthopedic implants, ~~in spite of~~ despite the profound changes in terms of composition, morphology and ~~micro-structure~~microstructure taking place during aging. In particular, a suitable application may be represented by temporary osteosynthesis devices~~,~~ commonly used to repair fractures

and therefore intended to be removed from the patient once the ossification process has taken place~~: with~~. In this respect, the use of a material cheaper than Ti and 316L simultaneously characterized by remarkable safety and stability~~,~~ could be a potential option.

Conclusions

In this work, the galvanic deposition of ~~coatings of~~ brushite-hydroxyapatite/polyvinyl acetate coatings on AISI304 steel was investigated~~,~~ by using~~, as anodes, Zinc and Aluminum~~zinc and aluminum as anodes. The presence of PVAc was confirmed by both Raman spectra and FT-IR/ATR. The SEM images showed that the size of the deposit clusters increases with time and the initial ~~concentration of~~ monomer concentration. X-ray diffraction and Raman spectroscopy ~~shows~~show the formation of a mixture of brushite and hydroxyapatite, enriching in the latter phase upon increasing the deposition temperature. Additionally, X-ray diffraction shows that the use of an aluminum anode leads to the formation of a low crystallinity coating. Similar results were obtained at higher deposition temperatures. After aging in SBF for 21 days, due to the dissolution/reprecipitation processes~~,~~ the coatings were ~~totally~~ completely converted ~~in~~into hydroxyapatite, which also includes Mg, K, Cl, and Na ions coming from SBF. Aged samples with PVAc obtained for longer deposition times also presented ~~also~~ a very low wettability, as confirmed by the contact angle measurements.

Corrosion tests, ~~carried out~~ conducted in an SBF solution for 21 days at 37°C, showed that the corrosion potential always remains ~~always~~ higher than the respective value for bare steel, while the corrosion current is slightly lower. These results demonstrate that the coatings act ~~like~~as physical barriers between the steel substrate and the SBF fluid, inhibiting their corrosion. Using aluminum as the sacrificial anode, after 21 days of aging in the SBF,

Formatted: Highlight

corrosion potentials of ~~about~~approximately 0.1 V (uncoated SS ~~about~~approximately -0.19 V) and a corrosion current density ~~of~~on the order of 10^{-7} A/cm^2 were measured, i.e., an order of magnitude lower than bare steel. The low corrosion rate was further demonstrated ~~by~~ via quantification~~,~~ through ICP-OES~~,~~ of the release of Fe, Ni and Co ions in SBF from coated and uncoated ~~substrate~~substrates after 21 days of aging. Very low values, far below the toxic level for human health, were found. The ~~C~~coatings have a high cytocompatibility, comparable to the control (pure cell culture medium), as ~~shoved~~shown by the cytotoxicity tests. In fact, through cell viability assays with MCT3-E1 osteoblastic cells, we ~~have~~ proved the ability of the coating to make ~~biocompatible~~ the SS support ~~biocompatible~~biocompatibility.

Acknowledgements

This work was supported by the University of Palermo. The authors would like to thank Prof. Giulio Ghersi from the STEBICEF Department of the University of Palermo for his technical support for biological tests. Francesco Lopresti ~~is~~ was funded by the European Social Fund (ESF) – PON A.I.M: Attraction and International Mobility_ AIM1845825 – 1. CUP: B74I18000260001.

References

Table I. Ca/P and Ca/Fe of BS/HA/PVAc coatings obtained ~~by~~ via galvanic deposition using aluminum as the anode and different ~~amount~~amounts of vinyl acetate (VAc) monomer at different times and temperatures. The mean standard deviation was 1%.

	Al, 24 h, T^{amb}		Al, 72 h, T^{amb}		Al, 24 h,50°C		Al, 72 h, 50°C	
VAc [mL]	Ca/P	Ca/Fe	Ca/P	Ca/Fe	Ca/P	Ca/Fe	Ca/P	Ca/Fe
0	1.37	12.31	1.59	22.81	1.57	27.2	1.69	34.57
0.75	1.42	14.23	1.61	23.86	1.66	29.01	1.59	35.84
1.5	1.39	13.47	1.57	21.66	1.65	26.4	1.62	32.98

Table II. Corrosion parameters at different aging times for samples obtained ~~by~~ via galvanic deposition at 50°C. For comparison, ~~also~~ the value of uncoated 304SS was also reported. The mean standard deviation was 2.3%.

	Time [day]					
25°C, 72 h, 0 mL VAc	0	1	7	14	21	SS 304
E_{corr} [V]	0.129	0.139	0.1717	0.099	0.078	-0.16
i_{corr} [A/cm^2]	2.05 E -06	1.26 E -06	2.15 E -06	1.64 E-06	2.36 E-06	3.92E-06

25°C, 72 h, 1.5 mL VAc	0	1	7	14	21	SS 304
E_{corr} [V]	0.14	0.088	-0.022	0.105	0,05	-0.16
i_{corr} [A/cm^2]	4.13 E -06	1.77 E -06	1.05 E -06	9.20 E-07	1.05 E-06	3.92E-06

50°C, 72 h, 1.5 mL VAc	0	1	7	14	21	SS 304
E_{corr} [V]	0.147	0.121	0.104	0.105	0.082	-0.16
i_{corr} [A/cm^2]	9.20E-07	1.87E-06	1.86E-06	1.10E-06	7.27E-07	3.92E-06

Table III. Ions concentration in SBF after 21 days of aging. For comparison, data for the as-prepared ~~as prepared~~ SBF solution are reported. The mean standard deviation was 0.5%.

	Fe	**Cr**	**Ni**	**Ca**	**P**
	Ppm	Ppm	Ppm	Ppm	Ppm
SBF (measured)	0	0	0	103.75	31.74
SBF (calculated)	0	0	0	105	31
304ss un-coated	0.037	0	0	82.22	25.44
24 h VAc 0mL	0	0.001	0.001	7.04	84.88
72 h VAc 0 mL	0	0.002	0.0005	3.86	141.26
24 h VAc 1.5 mL	0.022	0.001	0.005	11.96	55.22
72 h VAc 1.5 mL	0.017	0.003	0.001	5.84	111.1

Caption of figures

Figure 1. ~~Scheme of~~ gGalvanic deposition scheme of HA/BS/PVAc coatings on 304SS support.

Figure 2. SEM images of BS/HA/PVAc coatings obtained after 24 hours of galvanic deposition using ~~aluminium~~aluminum as the anode at different amounts of vinyl acetate monomer and temperatures.

Figure 3. XRD diffraction patterns of BS/HA/PVAc coatings obtained ~~by~~ via galvanic deposition by using ~~aluminium~~aluminum as the anode, at different amounts of vinyl acetate monomer and at different times and temperatures.

Figure 4. RAMAN spectra of BS/HA/PVAc coatings obtained ~~by~~ via galvanic deposition using ~~aluminium~~aluminum as the anode, at different amounts of vinyl acetate monomer and at different times and temperatures.

Figure 5. SEM image (a), XRD diffraction patterns (b) and RAMAN (c) spectrum of coatings obtained ~~by~~ via galvanic deposition using ~~aluminium~~aluminum as the anode after 21 days of aging in the SBF solution.

Figure 6. FT-IR/ATR spectra (a) and values of the angle contact of coatings obtained by galvanic deposition using ~~aluminium~~aluminum as the anode before and after 21 days of aging in the SBF solution.

Figure 7. Tafel plots of coatings obtained at (a) 25°C and (b) 50°C by galvanic deposition for 72 hours using ~~aluminium~~aluminum as the anode and with 1.5 mL of vinyl acetate during 21 days of aging in the SBF solution.

Figure 8. Impedance spectra of coatings obtained ~~by~~ via galvanic deposition at 50°C, using aluminum as anode and with 1.5 mL of vinyl acetate, during 21 days of aging in the SBF

solution.

Figure 9. Viability, measured by absorbance at 450 nm using CCK-8 kit, of MC3T3-E1 cells grown ~~with not treated~~in an untreated medium (positive control), naked sample~~-~~-treated (negative control) and coated ~~samples~~ sample-treated media. Asterisks indicate significant differences in cell viability ($P < 0.05$).

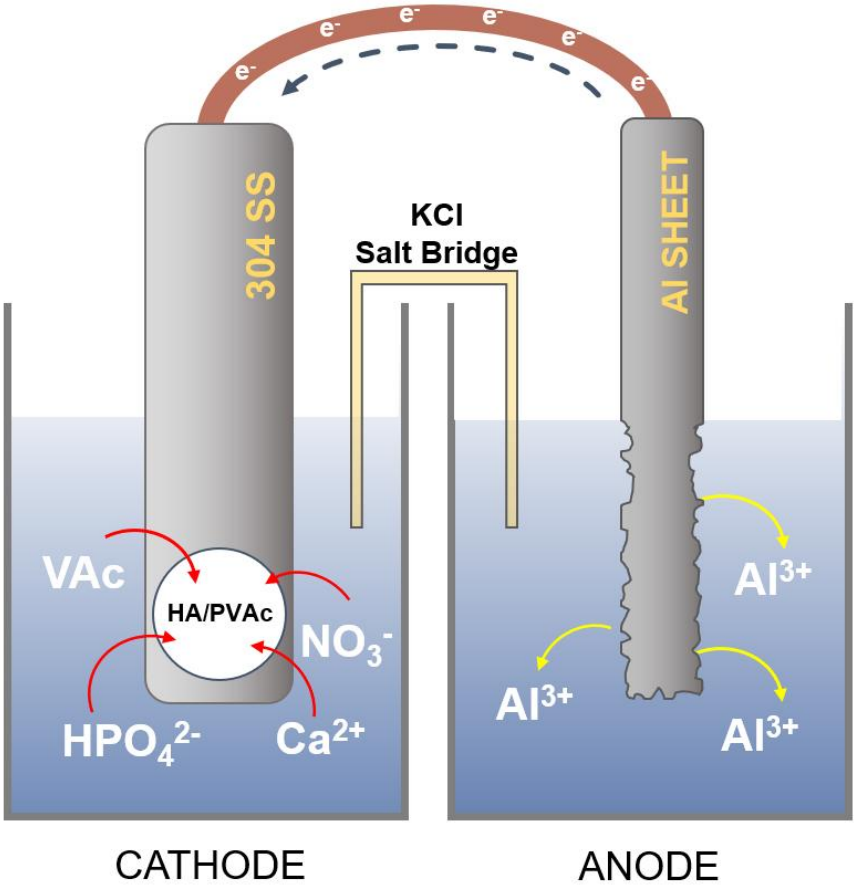
e-
e-
e-
e-
e-
e-
304 SS
KCl
Salt Bridge
Al SHEET
VAc
HA/PVAc
NO3-
HPO4 2-
Ca2+
Al3+
Al3+
Al3+
CATHODE
ANODE

Figure 1

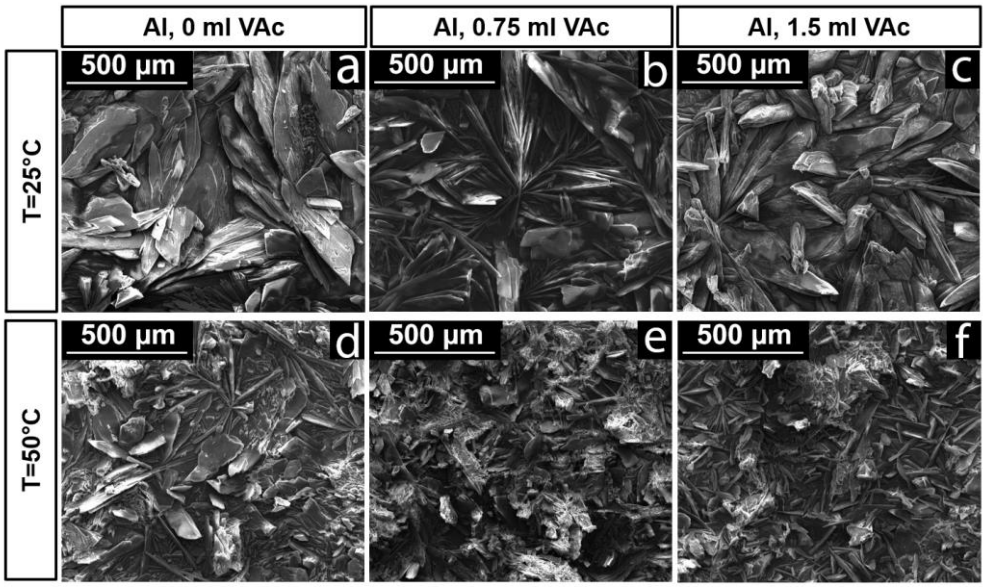

Figure 2

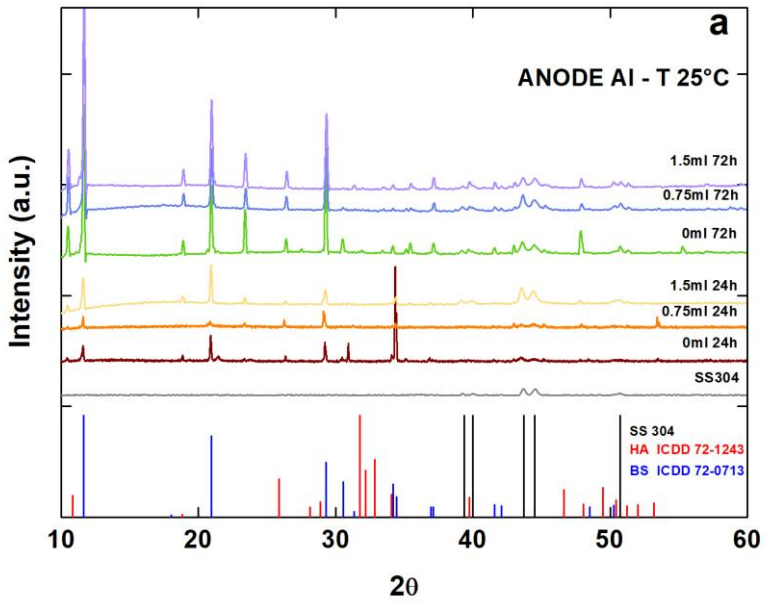
a
ANODE Al - T 25°C
1.5ml 72h
0.75ml 72h
0ml 72h
1.5ml 24h
0.75ml 24h
0ml 24h
SS304
SS 304
HA ICDD 72-1243
BS ICDD 72-0713
Intensity (a.u.)
10
20
30
40
50
60
2θ

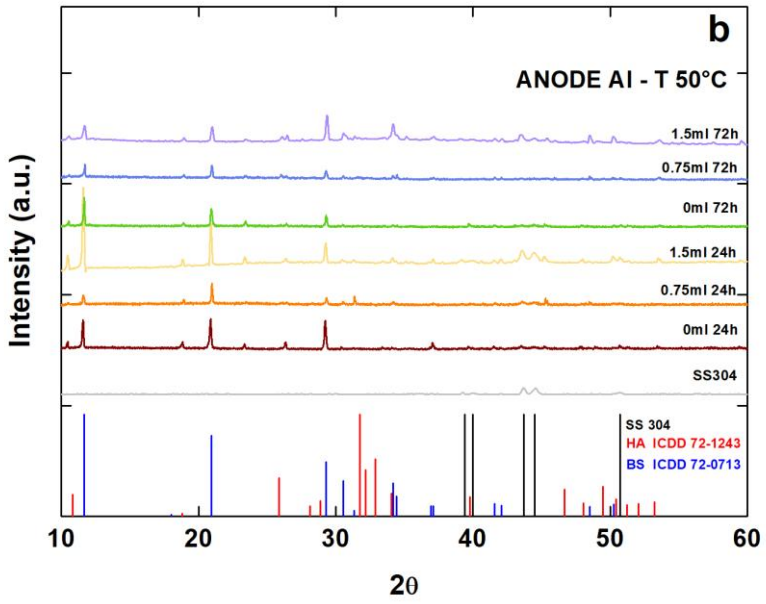
b
ANODE Al - T 50°C
1.5ml 72h
0.75ml 72h
0ml 72h
1.5ml 24h
0.75ml 24h
0ml 24h
SS304
SS 304
HA ICDD 72-1243
BS ICDD 72-0713
Intensity (a.u.)
10
20
30
40
50
60
2θ

Figure 3

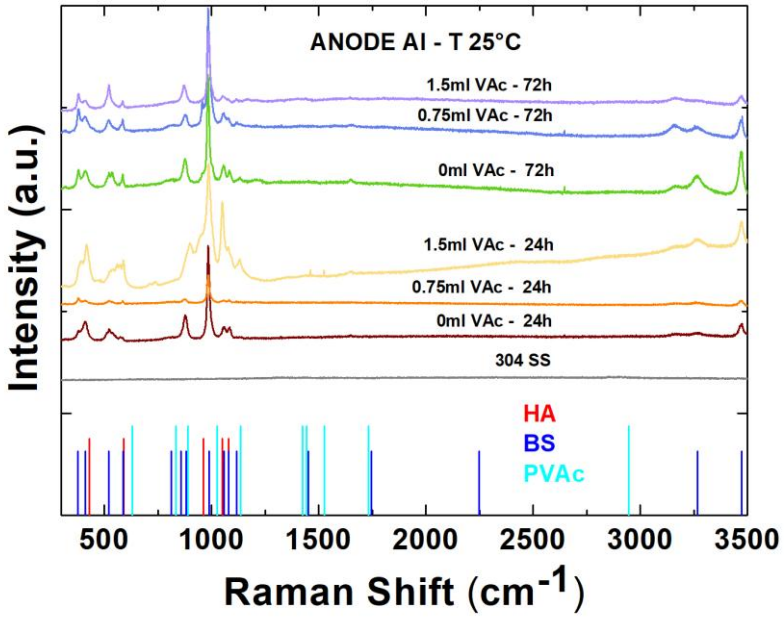
ANODE Al - T 25°C
1.5ml VAc - 72h
0.75ml VAc - 72h
0ml VAc - 72h
1.5ml VAc - 24h
0.75ml VAc - 24h
0ml VAc - 24h
304 SS
HA
BS
PVAc
Intensity (a.u.)
500
1000
1500
2000
2500
3000
3500
Raman Shift (cm-1)

Figure 4

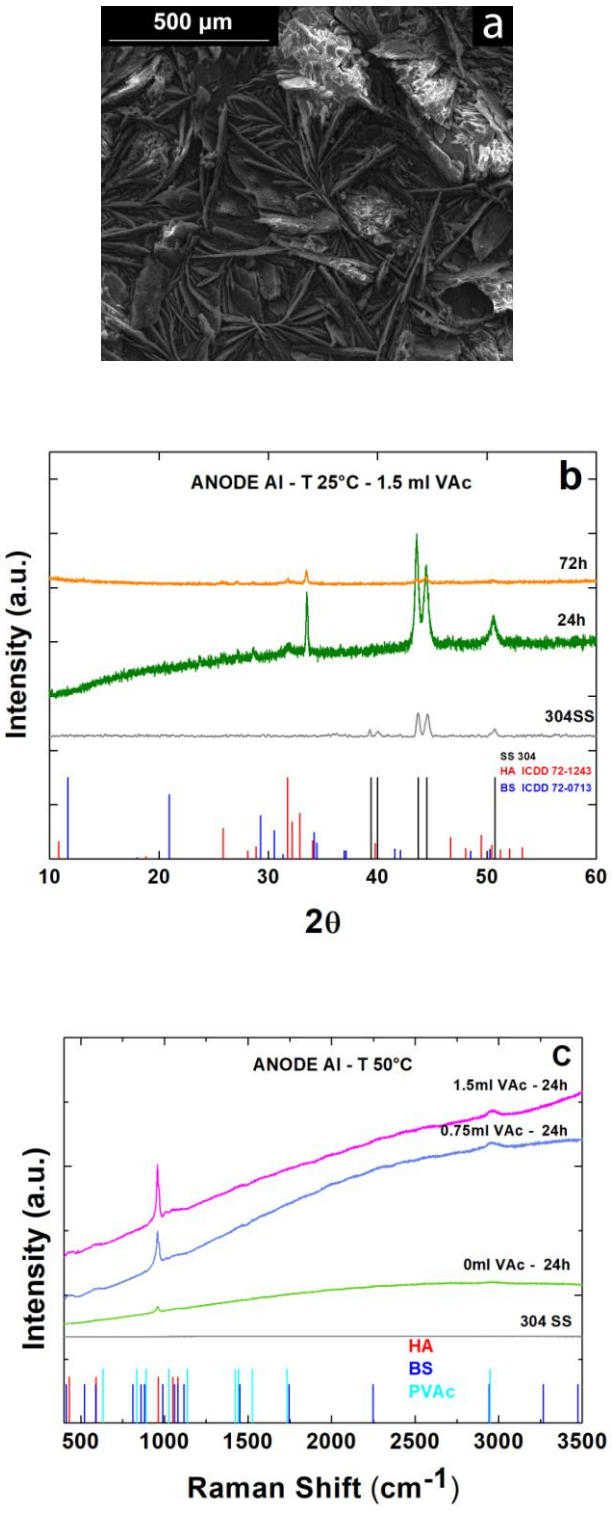
500 µm
a
ANODE Al - T 25°C - 1.5 ml VAc
b
72h
24h
304SS
SS 304
HA ICDD 72-1243
BS ICDD 72-0713
Intensity (a.u.)
10
20
30
40
50
60
2θ
ANODE Al - T 50°C
c
1.5ml VAc - 24h
0.75ml VAc - 24h
0ml VAc - 24h
304 SS
HA
BS
PVAc
Intensity (a.u.)
500
1000
1500
2000
2500
3000
3500
Raman Shift (cm-1)

Figure 5

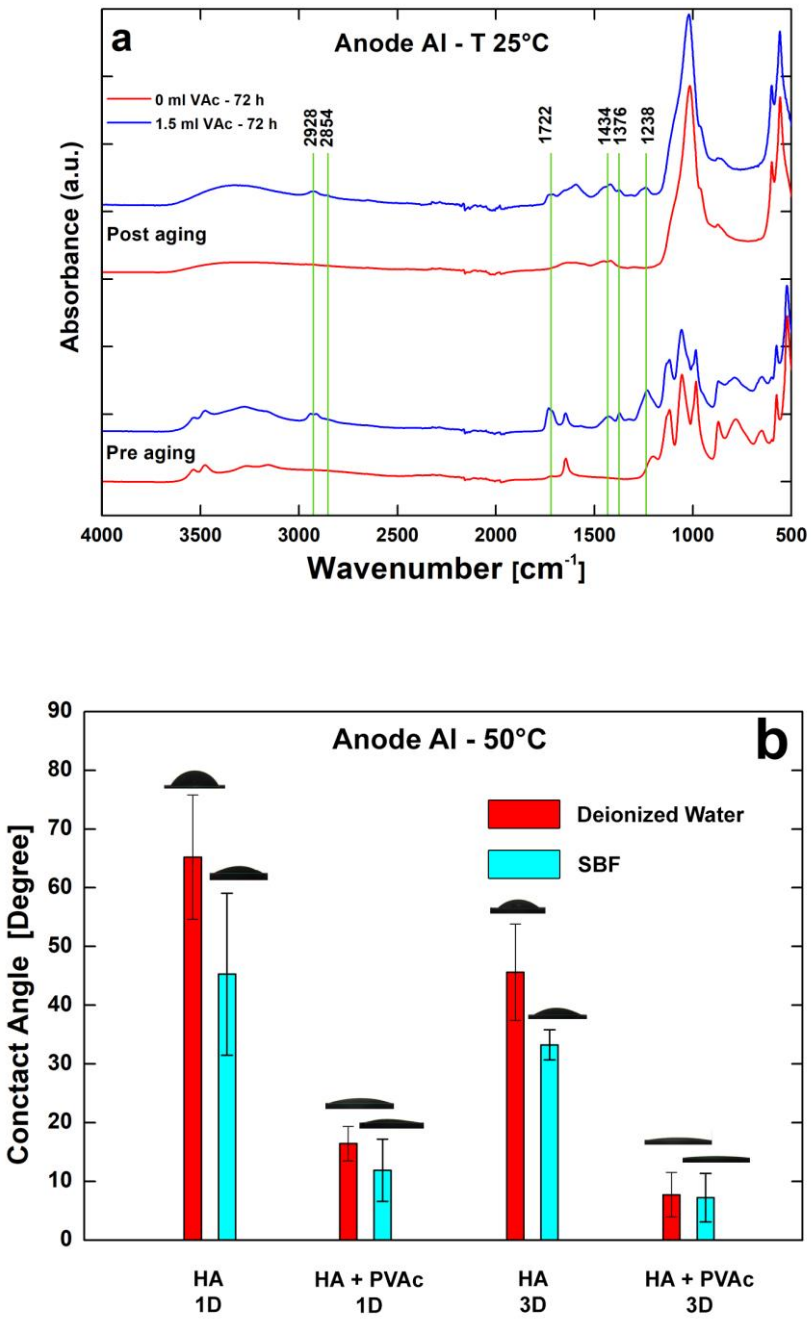
a
Anode Al - T 25°C
0 ml VAc - 72 h
1.5 ml VAc - 72 h
2928
2854
1722
1434
1376
1238
Post aging
Pre aging
Absorbance (a.u.)
4000
3500
3000
2500
2000
1500
1000
500
Wavenumber [cm-1]
b
Anode Al - 50°C
Deionized Water
SBF
Conctact Angle [Degree]
90
80
70
60
50
40
30
20
10
0
HA
1D
HA + PVAc
1D
HA
3D
HA + PVAc
3D

Figure 6

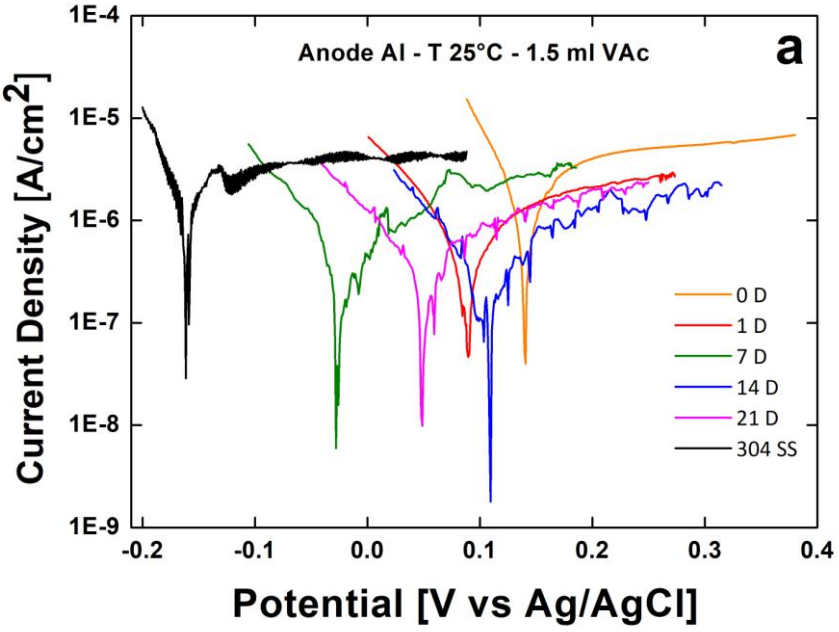
Anode Al - T 25°C - 1.5 ml VAc
a
Current Density [A/cm2]
1E-4
1E-5
1E-6
1E-7
1E-8
1E-9
-0.2
-0.1
0.0
0.1
0.2
0.3
0.4
Potential [V vs Ag/AgCl]
0 D
1 D
7 D
14 D
21 D
304 SS

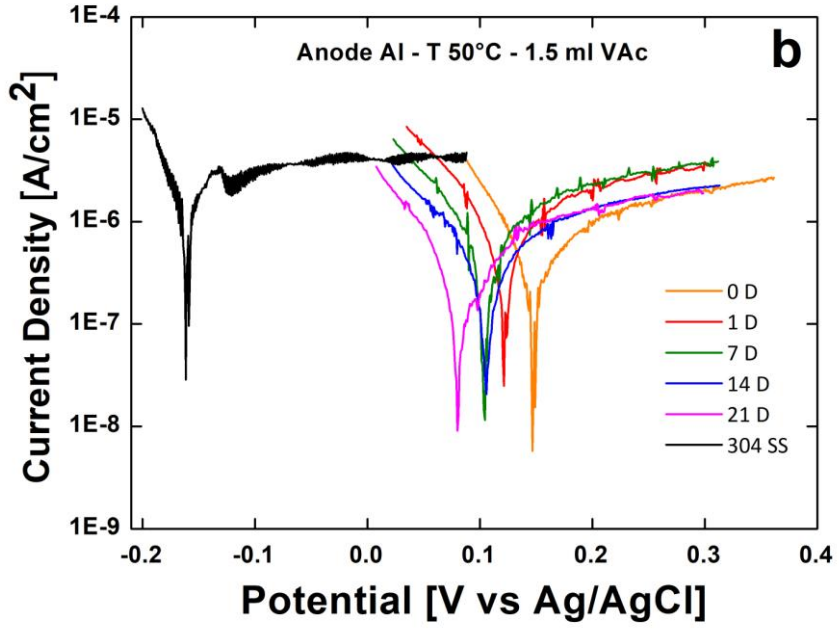
Anode Al - T 50°C - 1.5 ml VAc
b
Current Density [A/cm2]
1E-4
1E-5
1E-6
1E-7
1E-8
1E-9
-0.2
-0.1
0.0
0.1
0.2
0.3
0.4
Potential [V vs Ag/AgCl]
0 D
1 D
7 D
14 D
21 D
304 SS

Figure 7

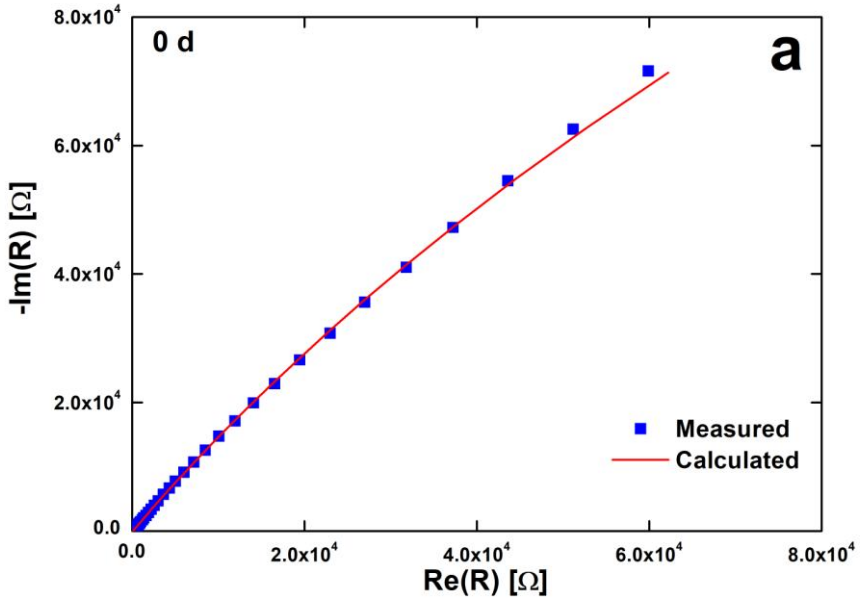
0 d
a
-Im(R) [Ω]
Re(R) [Ω]
Measured
Calculated
0.0
2.0x10^4
4.0x10^4
6.0x10^4
8.0x10^4

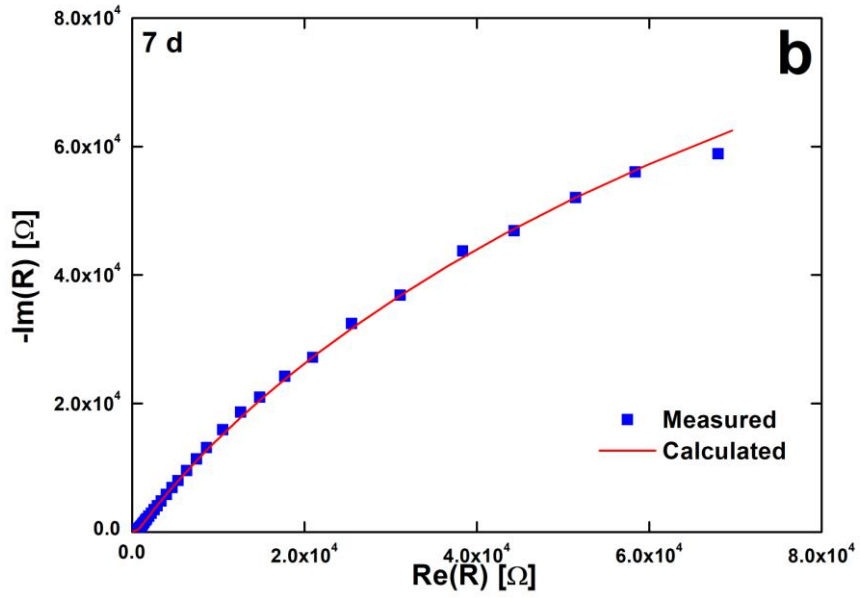
7 d
b
-Im(R) [Ω]
Re(R) [Ω]
Measured
Calculated
0.0
2.0x10^4
4.0x10^4
6.0x10^4
8.0x10^4

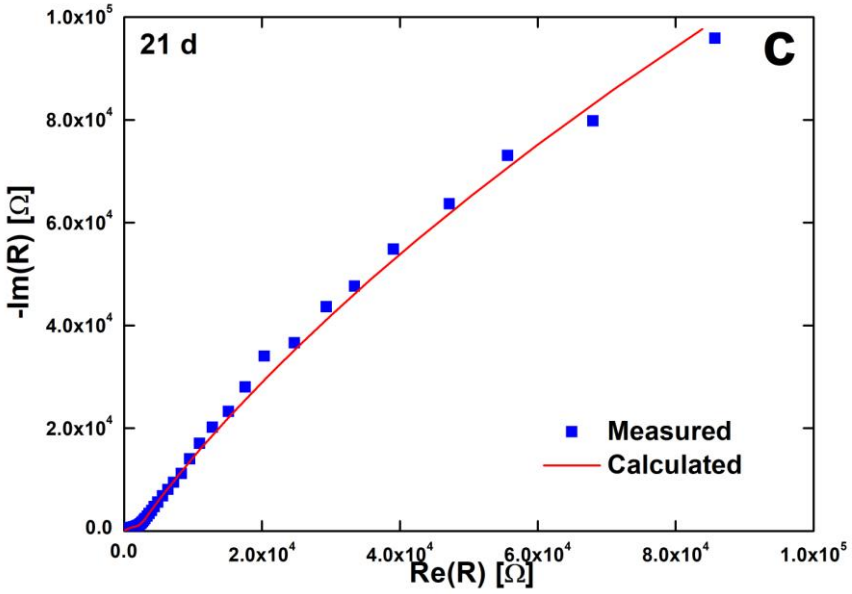
21 d
c
-Im(R) [Ω]
Re(R) [Ω]
Measured
Calculated
1.0x10^5
8.0x10^4
6.0x10^4
4.0x10^4
2.0x10^4
0.0

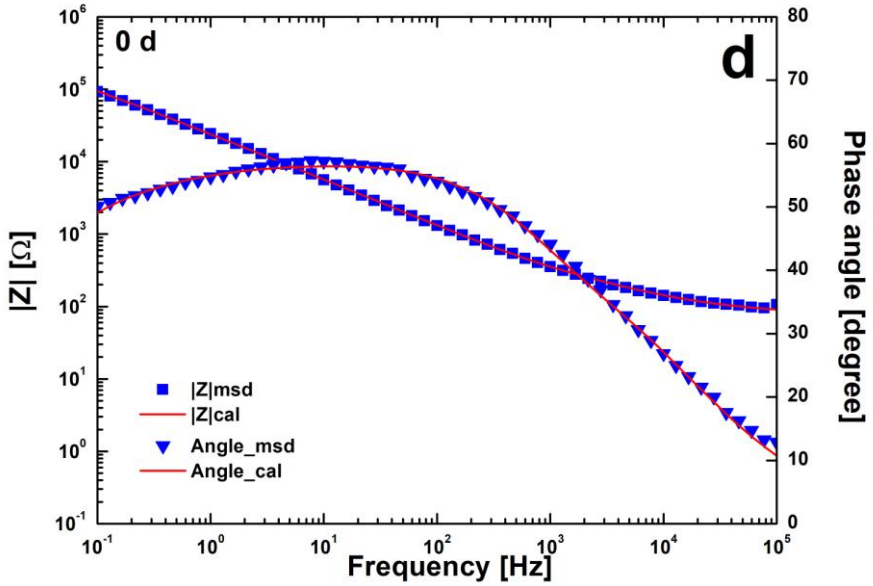
0 d
d
|Z| [Ω]
Phase angle [degree]
Frequency [Hz]
|Z|msd
|Z|cal
Angle_msd
Angle_cal

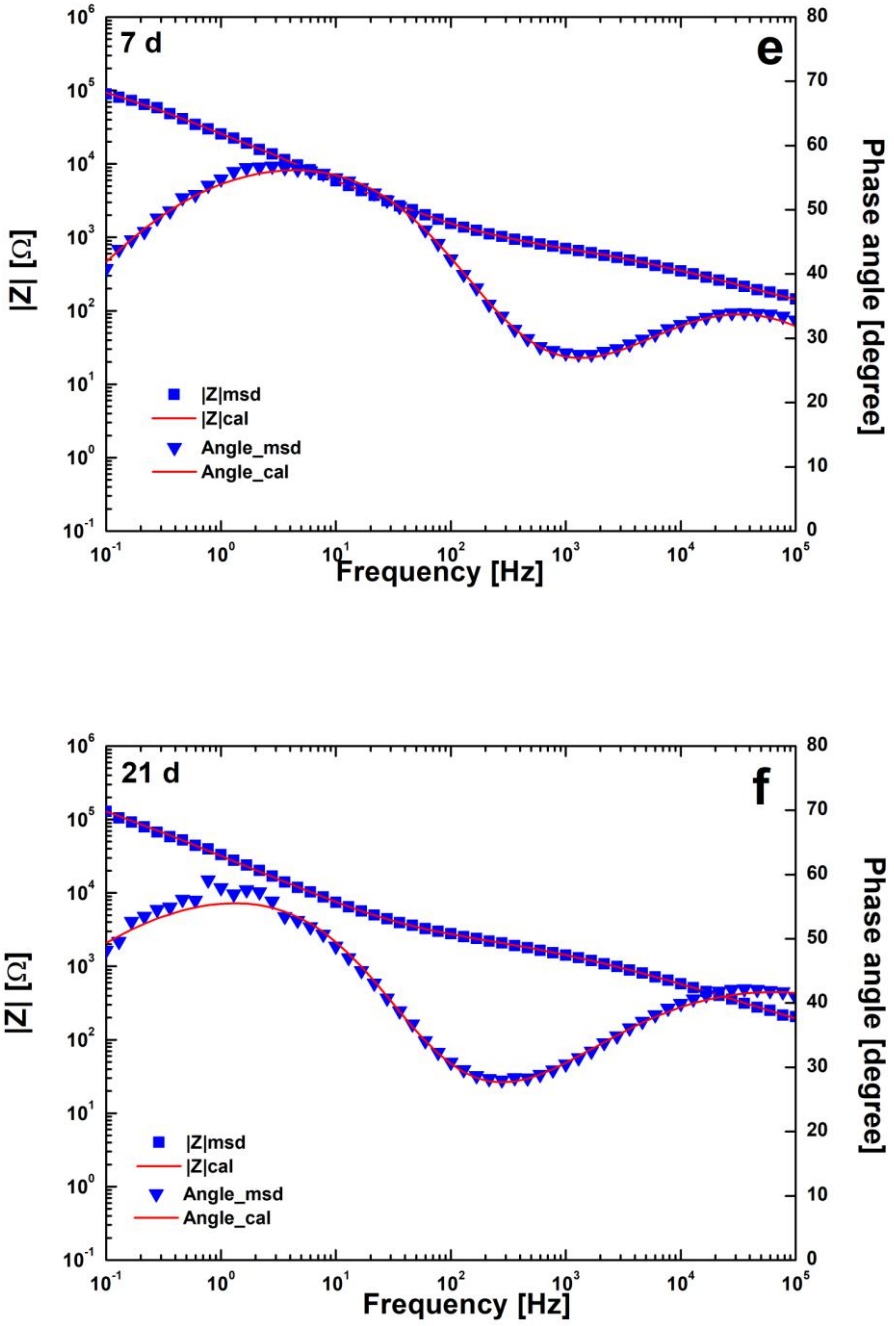
7 d
e
|Z|msd
|Z|cal
Angle_msd
Angle_cal
|Z| [Ω]
Phase angle [degree]
Frequency [Hz]
21 d
f
|Z|msd
|Z|cal
Angle_msd
Angle_cal
|Z| [Ω]
Phase angle [degree]
Frequency [Hz]

Figure 8 rev

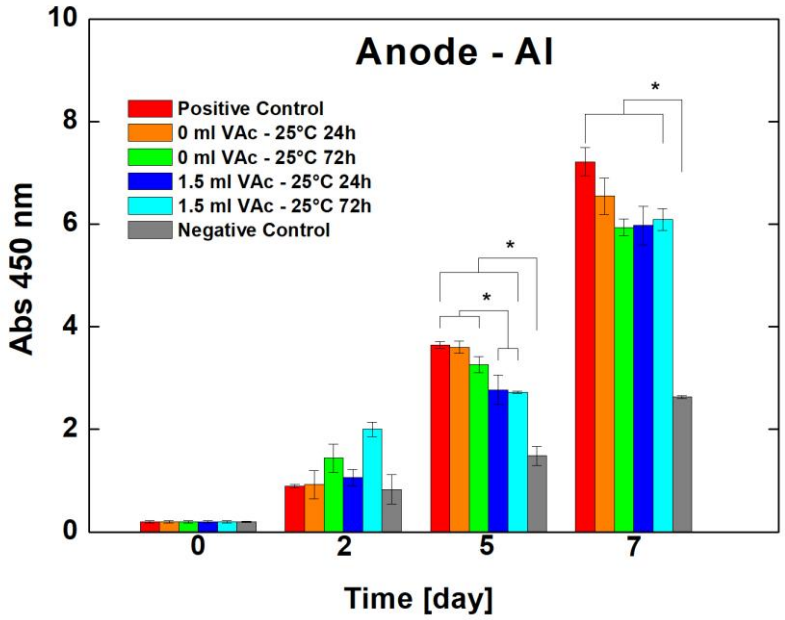
Anode - Al
Positive Control
0 ml VAc - 25°C 24h
0 ml VAc - 25°C 72h
1.5 ml VAc - 25°C 24h
1.5 ml VAc - 25°C 72h
Negative Control
Abs 450 nm
Time [day]
0
2
5
7
*
*
*

Figure 9 rev

Supplementary Material

Click here to download Supplementary Material: SupplementaryMaterial_REV.pdf

Calcium phosphate/polyvinyl acetate coatings on SS304 by galvanic co-deposition for orthopedic implant applications

I. Mendolia[1], C. Zanca[1], F. Ganci[1], G. Conoscenti[1], F. Carfì Pavia[1], V. Brucato[1,2], V. La Carrubba[1, 2, 3], F. Lopresti[1], S. Piazza[1], C. Sunseri[1], R. Inguanta[1,2 *]

[1]Dipartimento di Ingegneria, Università di Palermo, Viale delle Scienze - 90128 Palermo (Italy)

[2]INSTM Palermo Research Unit, Viale delle Scienze - 90128 Palermo (Italy)

[3]ATeN Center, Università di Palermo, Viale delle Scienze - 90128 Palermo (Italy)
[*]Corresponding Author E-mail Address: rosalinda.inguanta@unipa.it

CRediT authorship contribution statement

ISABELLA MENDOLIA: Investigation;

CLAUDIO ZANCA Investigation, Writing - Original Draft, Methodology;

FABRIZIO GANCI: Investigation;

GIOACCINO CONOSCENTI: Investigation, Methodology;

FRANCESCO CARFI' PAVIA: Investigation , Writing - Original Draft, Methodology;

VALERIO BRUCATO: Conceptualization, Supervisor;

VINCENZO LA CARRUBBA: Conceptualization, Writing- Reviewing and Editing, Supervisor;

FRANCESCO LOPRESTI: Investigation

SALVATORE PIAZZA: Supervisor;

CARMELO SUNSERI: Supervisor;

ROSALINDA INGUANTA: Conceptualization, Writing- Reviewing and Editing, Funding acquisition, Supervisor.

***Declaration of Interest Statement**

Declaration of interests

☒ The authors declare that they have no known competing financial interests or personal relationships that could have appeared to influence the work reported in this paper.

☐The authors declare the following financial interests/personal relationships which may be considered as potential competing interests: